Prediction of strong dichroism induced by x-rays carrying orbital momentum

Michel van Veenendaal[1,2] and Ian McNulty[2]
[1] *Dept. of Physics, Northern Illinois University, De Kalb, Illinois 60115*
[2] *Advanced Photon Source, Argonne National Laboratory, 9700 South Cass Avenue, Argonne, Illinois 60439*
(Dated: October 3, 2006)

We predict the presence of strong dichroic effects induced by x-ray beams carrying orbital angular momentum (OAM). Taking the difference between spectra obtained with positive and negative OAM states allows the separation of quadrupolar from dipolar transitions at, e.g., the transition-metal K edges, enabling the study of the unoccupied states in the absence of strong core-hole effects. We study the dependence of OAM-induced x-ray dichroism on different polarization vectors and derive sum rules that relate the integrated intensity to ground-state hole densities. Calculations of spectral line shapes for cuprates, manganites, and ruthenates confirm the strong OAM-induced dichroism and indicate the potential of this new spectroscopy in, e.g., the fields of orbital physics and magnetism.

PACS numbers: 78.70.Dm, 78.20.Fm

−Introduction. The field of singular optics has grown rapidly in the last 15 years stimulated by the work of Allen and co-workers [1] who demonstrated that beams with shaped profiles carry orbital angular momentum (OAM). So far, the focus has been on shaped beams in the visible region, which have been used for optical manipulation of molecules and nanoparticles [2], and the possible detection of faint astronomical objects [3]. The interaction between OAM carrying light and matter was studied for molecules in Laguerre-Gaussian and Bessel shaped laser modes [4–6]. More recently, the possibility of creating phase singularities or vortices with x-rays was demonstrated [7, 8]. In this Letter, we study absorption from core states using singular x-ray beams and predict the presence of significant dichroic effects induced by a reversal of the orbital angular momentum of the beam at a fixed polarization of the x-rays. Since core-level resonances are dominated by dipolar and quadrupolar transitions, the interpretation of these experiments is expected to be more straightforward than OAM-induced spectroscopy in the visible region. We discuss the dependence of OAM x-ray dichroism on the polarization of the x-rays and derive sum rules that relate the integrated intensity of the spectrum to ground-state properties. We discuss applications of OAM x-ray dichroism on cuprates, manganites, and ruthenates, highlighting this technique's sensitivity to changes in orbital occupancy.

−Theory. Inside the waist w of a singular x-ray beam, the vector potential $\mathbf{A}_n(\mathbf{r},t) = \mathbf{A}_n(\mathbf{r})e^{-i\omega t}$, for winding number n, wavevector $\mathbf{k}$ along the z axis, and energy $\hbar\omega$, is given by $\mathbf{A}_n(\mathbf{r}) = \hat{\mathbf{e}}A_n\left(\frac{\rho}{w}\right)^{|n|}e^{in\varphi+ikz}$ [1, 4–6], where $\hat{\mathbf{e}}$ is the polarization vector of the incoming x-rays, ρ the distance to the center of the beam, φ is the phase, and A_n the strength of the vector potential. X-ray spectroscopic line shapes are dominated by dipolar and quadrupolar transitions from the core level into the valence shell. We restrict ourselves here to winding numbers $n = \pm 1$, which are the most relevant for quadrupolar transitions, as we shall see below. To study the interaction between light and matter, we evaluate the matrix elements $\langle f|\frac{e}{m}\mathbf{p}\cdot\mathbf{A}(\mathbf{R}+\mathbf{r})|g\rangle \cong i\omega e\langle f|\mathbf{r}\cdot\mathbf{A}(\mathbf{R}+\mathbf{r})|g\rangle$, where $\mathbf{R}$ indicates the position of the atom with respect to the center of the beam. The photon energy $\hbar\omega$ is equal to the energy difference $E_f - E_g$ between the ground $|g\rangle$ and final states $|f\rangle$. For $n = \pm 1$, we write the vector potential as $i\omega\mathbf{A}_{\pm1} = \hat{\mathbf{e}}(E_\pm 1/w)(\rho_R e^{\pm i\Phi} + \rho e^{\pm i\varphi})e^{ikz}$, where $E_n = i\omega A_n$ is the electric field strength and ρ_R and Φ_R give the position of the atom in cylindrical coordinates. The position of the electrons with respect to the atom can be written as $\rho e^{\pm i\varphi} = \mp r_{\pm1}$, with r_q the spherical tensor components of $\mathbf{r}$. The x-ray absorption is

$$I_{\pm1}(\hat{\mathbf{e}},\omega) = \frac{e^2E_n^2}{w^2}\sum_{f,q}\hat{e}_q^2(\rho_R^2|\langle f|r_q|g\rangle|^2 + a_{q+n}|\langle f|r^{(2)}_{q\pm1}|g\rangle|^2)\delta(E_f - E_g - \hbar\omega), \quad (1)$$

with $a_{\pm1} = \frac{1}{3}$, $a_{\pm2} = \frac{2}{3}$, and $a_0 = \frac{1}{9}$. The first term on the right-hand side describes dipolar transitions related to the off-axis position of the atom; the second term describes quadrupolar transitions through the operator $r^{(2)}$. Note that the transferred momentum is $q \pm 1$ for winding numbers $n = \pm 1$. Quadrupolar transitions in singular x-ray beams arise from the radial dependence $\frac{r_{\pm1}}{w}$ of the vector potential and the matrix elements are proportional to $1/w$. This should be compared to electric quadrupole transitions for a plane wave that result from higher-order contributions, $e^{i\mathbf{k}\cdot\mathbf{r}} \cong 1 + i\mathbf{k}\cdot\mathbf{r}$, and where the matrix element is proportional to $k/2\sqrt{5}$.

The OAM dichroic signal for a particular polarization vector is obtained from the difference between $n = 1$ and -1 winding numbers, $I^{\rm dichroic}(\hat{\mathbf{e}},\omega) = I_1(\hat{\mathbf{e}},\omega) - I_{-1}(\hat{\mathbf{e}},\omega)$. Since the dipolar term does not depend on the OAM of the x-rays, it cancels and only the quadrupolar terms remain. Herein lies the strength of OAM x-ray dichroism. For example, for transition-metal compounds, the relevant physics is often related to the $3d$ states. However, for x-ray absorption at the transition-metal K

edge, the quadrupolar $1s \rightarrow 3d$ transitions are generally obscured by the presence of the strong dipolar $1s \rightarrow 4p$ transitions. Obviously, direct transitions into the $3d$ shell occur at the transition-metal L edges, but here the interpretation is often complicated by the presence of strong core-hole effects, such as the large spin-orbit coupling and Coulomb interactions between the core and valence shell. OAM-induced x-ray dichroism therefore provides unique insights into the unoccupied $3d$ projected density of states. Experiments are also possible at, e.g., the rare-earth L-edges, but here core-hole effects are present. The experiment gives for circular polarization vectors $\hat{\mathbf{e}}_{\pm 1}$

$$I^{\rm dichroic}(\hat{\mathbf{e}}_{\pm 1},\omega) = \pm\frac{2}{3}I^{(2)}_{\pm 2}(\omega) \mp \frac{1}{9}I^{(2)}_{0}(\omega), \qquad (2)$$

where the spectrum for a particular quadrupole component is given by

$$I^{(2)}_{k}(\omega) = \frac{e^2E_n^2}{w^2}\sum_f |\langle f|r^{(2)}_k|g\rangle|^2\delta(E_f - E_g - \hbar\omega). \qquad (3)$$

For linearly polarized light, we obtain

$$I^{\rm dichroic}(\hat{\mathbf{e}}_{x/y},\omega) = \frac{1}{3}[I^{(2)}_{2}(\omega) - I^{(2)}_{-2}(\omega)]. \qquad (4)$$

−Sum rules. Sum rules that relate the integrated intensity of a spectrum to ground-state expectation values of operators, such as the number of holes and the orbital moment, have played an important role in the development of x-ray magnetic dichroism [9]. Let us consider the $1s \rightarrow 3d$ absorption edge in transition-metal systems. In second quantization, the transition matrix elements are $\langle d|r^{(2)}_q|s\rangle = \frac{1}{\sqrt{5}}(d||r^{(2)}||s)\sum_\sigma \langle d|d^\dagger_{q\sigma}s_{0\sigma}|s\rangle$, where $d^\dagger_{m\sigma}$ and $s^\dagger_{m\sigma}$ create an electron with orbital moment m and spin $\sigma = \pm\frac{1}{2}$ in the $3d$ and $1s$ shells, respectively; $(d||r^{(2)}||s) = \sqrt{3}\int drr^2R_{3d}(r)rR_{1s}(r)$ is the reduced matrix element, where R_{3d} and R_{1s} are the radial parts of the $3d$ and $1s$ orbitals, respectively. For clarity, the constant scaling factor $(d||r^{(2)}||s)\frac{eE_n}{w}$ will be set to unity. The integrated intensities are

$$\int I^{\rm dichroic}(\hat{\mathbf{e}}_{\pm 1},\omega)d\omega = \pm\frac{2}{15}\langle \underline{n}_{\pm 2}\rangle \mp \frac{1}{45}\langle \underline{n}_0\rangle, \qquad (5)$$

where the integration goes over the $1s \rightarrow 3d$ transitions; $\langle \underline{n}_m\rangle$ is the hole density in the $3d$ orbital with angular momentum m. For transition-metal compounds, it is often more convenient to use real orbitals instead of atomic-like orbitals, giving

$$\int I^{\rm dichroic}(\hat{\mathbf{e}}_{\pm 1},\omega)d\omega = \pm\frac{1}{15}(\langle \underline{n}_{x^2-y^2}\rangle + \langle \underline{n}_{xy}\rangle) \mp\frac{1}{45}\langle \underline{n}_{3z^2-r^2}\rangle) + \frac{i}{15}\langle d_{x^2-y^2}d^\dagger_{xy} - d_{xy}d^\dagger_{x^2-y^2}\rangle. \qquad (6)$$

When using linearly polarized light, the sum rule is

$$\int I^{\rm dichroic}(\hat{\mathbf{e}}_{x/y},\omega)d\omega = \frac{1}{15}(\langle \underline{n}_2\rangle - \langle \underline{n}_{-2}\rangle) = \frac{i}{15}\langle d_{x^2-y^2}d^\dagger_{xy} - d_{xy}d^\dagger_{x^2-y^2}\rangle. \qquad (7)$$

−Applications: Cuprates. To obtain a better understanding of this new spectroscopy, let us consider the simple system of a divalent copper atom. In spherical symmetry with a magnetic field along the z axis (SO_2), the ground state has a hole in the orbital with $m = -2$ and $\sigma = -\frac{1}{2}$, see the bottom inset in Fig. 1(a). Transitions can only be made for $n + q = -2$, requiring right circular polarization $\mathbf{e}_{-1}$ and a winding number $n = -1$. Since the OAM dichroic signal measures $I_1 - I_{-1}$, the signal is negative with an integrated intensity proportional to the hole density in the $m = -2$ orbital, i.e., $\int I^{\rm dichroic}(\hat{\mathbf{e}}_{-1},\omega)d\omega \sim -\frac{2}{15}\langle \underline{n}_{-2}\rangle$. The absorption for left circular and linear polarization are zero and the average of left and right circularly polarized light, respectively.

The spectra change significantly for a copper atom in a local D_{4h} symmetry, see Fig. 1(b). This corresponds to a Cu atom surrounded by an octahedron of ligand atoms elongated in the z-direction, a typical situation in cuprates, such as the high-T_c superconductors. In the absence of $3d$ spin-orbit coupling, the ground state is a hole in the $x^2 - y^2$ orbital, and the spectra for left and right circularly polarized light are equal with an integrated intensity $\int I^{\rm dichroic}(\omega)(\hat{\mathbf{e}}_{\pm 1},\omega)d\omega = \pm\frac{1}{15}\langle n_{x^2-y^2}\rangle$. The signal for linearly polarized light would be zero. However, a small signal is observed, see Fig. 1(b), due to the spin-orbit coupling, which, to lowest order, couples $x^2 - y^2$ with the t_{2g} orbitals, giving a ground state $|g\rangle = |x^2-y^2\ \downarrow\rangle - \frac{i\zeta}{E_{xy}}|xy\ \downarrow\rangle + \frac{\zeta}{2E_{yz/zx}}(i|yz\ \uparrow\rangle + |zx\ \uparrow\rangle)$, where ζ is the strength of the spin-orbit coupling, and E_{xy} and $E_{yz/zx}$ is the on-site energy for a hole in the xy and yz/zx orbitals, respectively, relative to that for a hole in the $x^2 - y^2$ orbital, where, For Fig. 1, $\zeta = 0.13$ eV and $E_{xy} = E_{yz/zx} = 1.5$ eV. From this, we obtain that $\langle \underline{n}_{\mp 2\downarrow}\rangle = \frac{1}{2}\left(1 \pm \frac{\zeta}{E_{xy}}\right)^2$. For the OAM dichroic signal with linearly polarized light, we have $\frac{i}{15}\langle d_{x^2-y^2}d^\dagger_{xy} - d_{xy}d^\dagger_{x^2-y^2}\rangle = -2\zeta/E_{xy}$. The signal with

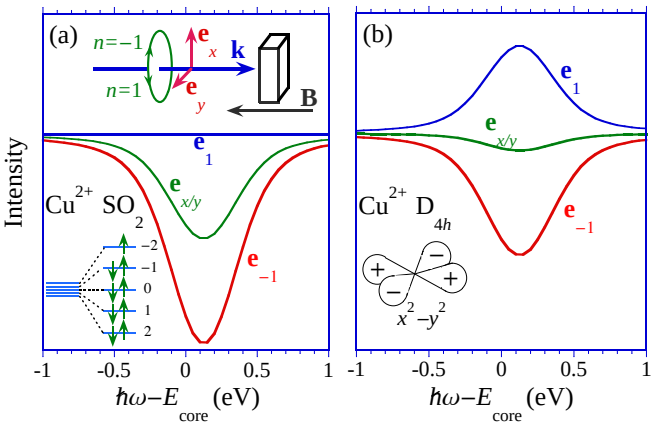

FIG. 1: (color online) (a) The dichroic OAM signal for circular ($\mathbf{e}_1$ and $\mathbf{e}_{-1}$) and linear ($\mathbf{e}_{x/y}$) polarization of the incoming x-rays for a divalent copper atom in spherical symmetry with a magnetic field along the z axis. (b) The same, but for a Cu^{2+} atom in a crystal field with D_{4h} symmetry.

linearly polarized light is, to lowest order, about $2\zeta/E_{xy}$ smaller than the OAM dichroic signals with circularly polarized light. Note, that in an antiferromagnetic system, the spin-orbit related part cancels.

–Manganites. Let us now turn our attention to some applications where the characteristics of OAM x-ray dichroism can be really beneficial. As described in the previous sections, OAM-induced dichroism measures the difference in occupation between the atomic orbitals with $m = \pm 2$ and $m = 0$. Therefore, this technique is extremely sensitive to relative changes in the occupancy of the e_g orbitals $3z^2 - r^2$ and $x^2 - y^2$. This interplay between different e_g orbitals plays a crucial role in manganites, such as $R_{1-x}A_x\mathrm{MnO_3}$ and $R_{2-x}A_x\mathrm{MnO_4}$, where R is a trivalent rare-earth ion and A is a divalent alkaline ion. These systems have received significant attention in recent years due to the strong dependence of their resistivity on magnetic field, known as colossal magnetoresistance [10]. Although double-exchange between the Mn t_{2g}^3 core spins by delocalized e_g electrons can cause magnetoresistance [11], this mechanism is often considered insufficient to explain the change of several orders of magnitude in conductivity [12]. To account for this, the presence of a strong dynamic Jahn-Teller coupling was suggested causing a crossover from an insulating polaronic to a metallic regime. These Jahn-Teller distortions have different orientations and have been studied with x-ray spectroscopy. Although conventional x-ray dichroism is a powerful technique, the interpretation of the spectral line shape at transition-metal L and M edges is often

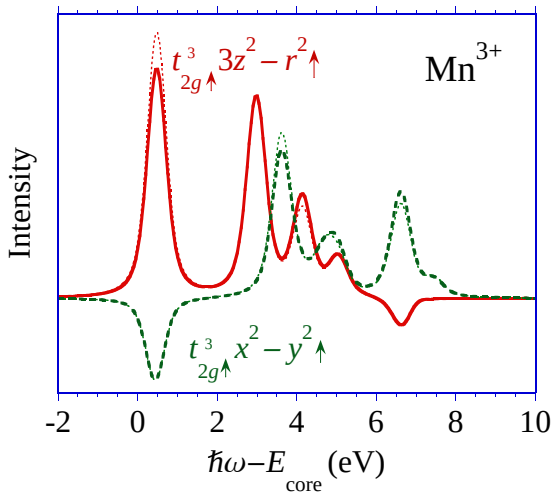

FIG. 2: (color online) OAM x-ray dichroism spectra for a Mn^{3+} ion for two different ground states. The incoming polarization vectors are $\hat{\mathbf{e}}_1$ (solid and dashed) and $\hat{\mathbf{e}}_{-1}$ (dotted). For a $t_{2g}^3 \uparrow 3z^2 - r^2 \uparrow$ ground state (red solid line), the excitations close to the absorption edge are a result of excitations into the $x^2 - y^2 \uparrow$ orbital leading to a large positive peak . One the other hand, for a $t_{2g}^3 \uparrow x^2 - y^2 \uparrow$ ground state (green dashed line), the excitations close to the edge are into the $3z^2 - r^2 \uparrow$ states and therefore show up as a negative peak in the OAM x-ray dichroism.

complicated due to the large core-hole spin-orbit coupling and Coulomb multiplets between the core hole and the valence shell [13]. The $1s$-$3d$ exchange interaction is only 0.06 eV [14], and the Mn K edge x-ray absorption reflects more closely the unoccupied density of states.

Figure 2 shows the difference in OAM x-ray dichroic spectral lines shapes for $S = 2$ ground states with $t_{2g}^3 \uparrow 3z^2 - r^2 \uparrow$ and $t_{2g}^3 \uparrow x^2 - y^2 \uparrow$ configurations. A clear distinction between the two ground states can be observed just above the absorption edge. This peak corresponds to the addition of a spin-up electron creating a $t_{2g\uparrow}^3 e_{g\uparrow}^2$ ($S = 5/2$) state. There is a distinct difference between the two spectra. For the ground state with a $3z^2 - r^2$ electron, excitations are made into the $x^2 - y^2 \uparrow$ orbital. Since $x^2 - y^2$ is a linear combination of $m = 2$ and -2 atomic-like orbitals, the peak is positive. On the other hand, for a ground state with an electron in $x^2 - y^2 \uparrow$, a high-spin state is created by adding a $3z^2 - r^2 \uparrow$ ($m = 0$) electron, and the peak intensity in the dichroism is negative. The spectral features at 2 eV and higher above the absorption edge are a result of quartet ($S = 3/2$) dd multiplet states. At energies greater than 6 eV above the edge, the dichroic signal is opposite to that just above the edge. These multiplets are $t_{2g}^3(^4A_2)e_g^2(\Gamma)$ with $\Gamma =^1 A_1,^1 E$ (O_h notation), which are at high energy since they consist of states where the added e_g electron is in the same orbital as the e_g electron in the ground state, i.e., $x^2 - y^2 \uparrow, x^2 - y^2 \downarrow$ and $3z^2 - r^2 \uparrow, 3z^2 - r^2 \downarrow$.

–Ruthenates. The selective probing of the $m = \pm 2$ components of the atomic orbitals also allows the study of changes in the relative occupations of the t_{2g} orbitals. With OAM x-ray dichroism along the z axis with circularly polarized light, excitations can be made into the planar xy orbitals, which are a linear combinations of the $m = \pm 2$ atomic-like orbitals, but not into the out-of-plane t_{2g} orbitals yz and zx, which consist of the $m = \pm 1$ spherical harmonics. A system where strong changes in the t_{2g} occupations have been observed are the ruthenates, such as Ca_2RuO_4 [15]. Hybridization is large for the ruthenates systems and calculations are done for a RuO_6 cluster with hybridization matrix elements $(pd\pi) = -0.45(pd\sigma) = 1.4$ eV, a charge-transfer energy of 4 eV, and an on-site Coulomb interaction of 3 eV. Atomic spin-orbit coupling and Coulomb multiplet parameters are used [14]. The ruthenates have a strong crystal-field splitting consisting of a point-charge crystal field, which we take 1.5 eV, and the strong hybridization. This results in a low-spin t_{2g}^4 ground state. Here, we are interested how the in-plane versus out-of-plane t_{2g} occupation affects the OAM x-ray dichroism. To vary the occupation, a crystal-field splitting between the xy and yz/zx orbitals, $E_{yz/zx} - E_{xy}$, was introduced. Figure 3(a) shows the OAM x-ray dichroism for $\hat{\mathbf{e}}_1$. The spectra for $\hat{\mathbf{e}}_{-1}$ are very similar. Due to the large crystal-field splitting between the e_g and t_{2g} orbitals, we can often clearly separate excitations into the xy orbitals (< 2 eV) and excitations into the $x^2 - y^2$ and $3z^2 - r^2$ orbitals (> 2 eV). Figure 3 shows the integrated intensities as a function

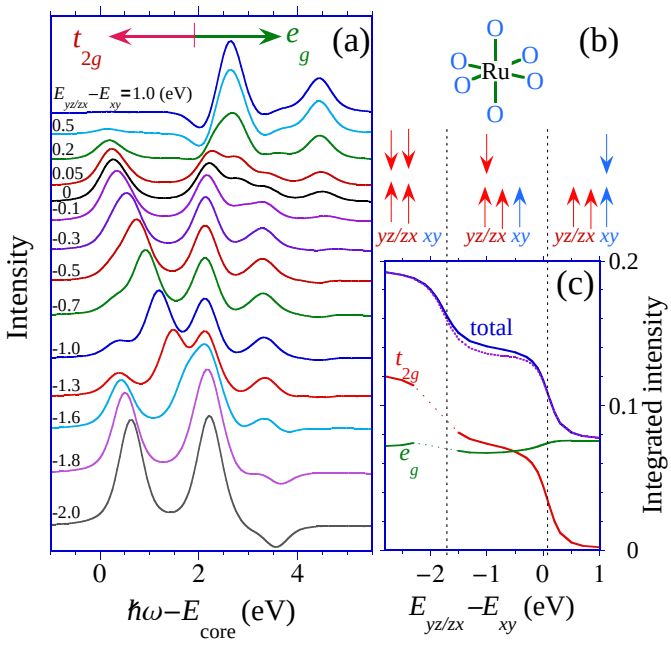

FIG. 3: (color online) (a) OAM x-ray dichroism for ruthenates calculated for a RuO_6 cluster, see (b), for a splitting of the t_{2g} orbitals given by $E_{yz/zx} - E_{xy}$ as given in the Figure. (c) The integrated intensity of the spectrum as a function of $E_{yz/zx} - E_{xy}$. The solid line indicated total (blue, solid) gives the total integrated intensity for an incoming polarization vector $\hat{\mathbf{e}}_1$. Also shown is the intensity of $\hat{\mathbf{e}}_{-1}$ (purple, dotted). The curves indicated t_{2g} (red) and e_g (green) give the integrated intensities for the low-energy states (< 2 eV) and the high-energy states (> 2 eV). The dotted part indicates the region where the low- and high-energy states are difficult to separate.

of $E_{yz/zx} - E_{xy}$. We see a decrease of the total intensity. From the separation of the integrated intensity into low- and high-energy regions, we can clearly see that the change in intensity is mainly a result of the decrease in intensity in the low-energy region related to excitations into the xy orbitals. We can clearly distinguish three plateaus, corresponding to ground states with predominantly $yz\uparrow\, yz\downarrow\, zx\uparrow\, zx\downarrow$ (2 xy holes, corresponding to a integrated intensity of $\frac{2}{15}$), $yz\uparrow\, zx\uparrow\, (yz/zx)\downarrow\, xy\uparrow$ (1 xy hole), and $(yz/zx)\uparrow\, (yz/zx)\downarrow\, xy\uparrow\, xy\downarrow$ (no xy holes) character, see Fig. 3(b). Note that the integrated intensity basically follows the xy hole densities. The transitions between the different ground states is smooth due to the $4d$ spin-orbit coupling ($\zeta = 0.16$ eV).

−Conclusions. We have shown the possibility of performing quadrupolar x-ray dichroism induced by the orbital angular momentum of the light. Taking the difference between negative and positive OAM states removes the OAM-independent electric multipole transitions and dipolar transitions related to the off-axis position of the beam. The signal of the quadrupolar OAM-induced signal can be enhanced with respect to the other contributions by the use of x-ray OAM beams approaching the scale of atomic orbital dimensions. Diffractive optics for focusing intense coherent x-ray beams to the nanometer scale have been demonstrated [16], and focusing singular x-ray optics designed along similar principles are feasible [17, 18]. OAM-induced x-ray dichroism provides a unique way to study the electron-addition states close to the Fermi level in the absence of a large core-hole spin-orbit coupling and strong multiplet effects between the core and valence states. In particular, the spectral line shape is very sensitive to changes in orbital occupancies, such as in plane-out of plane redistributions of electron densities in the e_g orbitals in manganites and the t_{2g} orbitals in ruthenates. Finally, we suggest that this approach might be applied to study x-ray OAM-induced dichroism effects in resonant scattering experiments.

Discussions with Andreas Menzel and Serkan Erdin are acknowledged. This work was supported by the U.S. Department of Energy (DOE), DE-FG02-03ER46097, and NIU's Institute for Nanoscience, Engineering, and Technology under a grant from the U.S. Department of Education. Work at Argonne National Laboratory was supported by the U.S. DOE, Office of Science, Office of Basic Energy Sciences, under contract W-31-109-ENG-38.

[1] L. Allen *et al.*, Phys. Rev. A **45**, 8185 (1992).
[2] For a review, see D. G. Grier, Nature **424**, 810 (2003).
[3] G. A. Swartzlander, Opt. Lett. **26**, 497 (2001).
[4] M. Babiker *et al.*, Phys. Rev. Lett. **89**, 143601 (2002).
[5] A. Alexandrescu, E. Di Fabrizio, and D. Cojoc, J. Opt. B: Quantum Semiclass. Opt. **7**, 87 (2005).
[6] A. Alexandrescu, D. Cojoc, and E. Di Fabrizio, Phys. Rev. Lett. **96**, 243001 (2006).
[7] A. G. Peele *et al.*, Opt. Lett. **27**, 1752 (2002); A. G. Peele *et al.*, J. Opt. Soc. Am. A **21**, 1575 (2004)
[8] I. McNulty, S. Rehbein, S. Eisebitt, A. Menzel, C. Günther, and F. Senf, Appl. Phys. Lett., in press.
[9] B. T. Thole, P. Carra, F. Sette, and G. van der Laan, Phys. Rev. Lett. **68**, 1943 (1992); P. Carra, B. T. Thole, M. Altarelli, and X. Wang, *ibid.* **70**, 694 (1993).
[10] For a review, see M. B. Salamon and M. Jaime, Rev. Mod. Phys. **73**, 583 (2001).
[11] C. Zener, Phys. Rev. **82**, 403 (1951); P. W. Anderson and H. Hasegawa, Phys. Rev. **100**, 675 (1955).
[12] A. J. Millis, P. B. Littlewood, and B. I. Shraiman, Phys. Rev. Lett. **74**, 5144 (1995).
[13] D. J. Huang *et al.*, Phys. Rev. Lett. **92**, 087202 (2004).
[14] R. D. Cowan, *The Theory of Atomic Spectra* (University of California Press, Berkeley, 1981).
[15] T. Mizokawa *et al.*, Phys. Rev. Lett. **87**, 077202 (2001).
[16] H.C. Kang, *et al.*, Phys. Rev. Lett. **96**, 127401 (2006).
[17] D. Cojoc *et al.*, Microelectronic Engineering **83**, 1360 (2006).
[18] S. Rehbein, I. McNulty, A. Menzel, C. Günther, A. Peele, M. DeJonge, C. Rau, and S. Eisebitt, to be published.